The Maximum Allowable Time Step for the Shallow Water α Model and Its Relation to Time-Implicit Differencing

B. A. WINGATE

Computer and Computational Sciences and Center for Nonlinear Studies, Los Alamos National Laboratory, Los Alamos, New Mexico

(Manuscript received 9 September 2003, in final form 20 April 2004)

ABSTRACT

This work investigates the numerical time stability of the Lagrangian-averaged shallow water α model (SW-α). The main result is an analytical estimate for the maximum allowable time step. This estimate shows that as the grid is refined the time step becomes independent of the mesh spacing and instead depends on the length scale, α, a parameter of the model. The α model achieves this result through changes in the equations of motion that reduce the frequency of the linear waves at high wavenumbers. This type of reduction in the frequency of high-wavenumber waves is also a characteristic of time-implicit numerical methods. Consequently, an analogy is drawn between the two by comparing the numerical method's modified equation to the partial differential equation of the α model. Fourier analysis and numerical simulations are also used to compare a third-order Adams–Bashforth α model simulation to the well-known implicit numerical method of Dukowicz and Smith.

1. Introduction

The Navier–Stokes α (NS-α) equations, introduced in Holm et al. (1998), filter the fluid motion that occurs below some length scale, α. The length scale, α, is the average correlation length associated with the covariance tensor $\overline{\xi\xi}$ for the fluctuating displacement $\xi(\mathbf{x}, t) = \mathbf{x}(\mathbf{x}_0, t) - \overline{\mathbf{x}}(\mathbf{x}_0, t)$ of a Lagrangian fluid parcel trajectory away from its Lagrangian mean trajectory with the same fluid label $\mathbf{x}_0$. In fact, it is temporal averaging in Hamilton's principle that leads to a dynamical spatial filtering in the resulting equations of motion. The longer the time averages over the Lagrangian mean trajectories, the larger the length scale α. This connection between the time and space averaging is discussed in Holm (1999).

In practice, α represents the smallest active scale in the solution below which the dynamics at smaller scales are regarded as passive. These small scales, instead of being diffused as occurs in many Eulerian averaging methods, are ''dragged,'' or ''swept,'' by the fluid motion of the large scales.

The solution behavior and turbulence properties of various forms of the α model have been explored in numerous numerical simulations. The NS-α model equations were discussed in Chen et al. (1998, 1999a,b). The corresponding modifications of the quasigeostrophic equations (QG-α) were tested numerically in Holm and Nadiga (2003) and Nadiga and Margolin (2001). The 2D Euler-α equations were investigated in Nadiga and Shkoller (2001), and the shallow water version of the α model was studied in D. Holm et al. (2003, unpublished manuscript). The effects of the α model on turbulent spreading of shear layers were compared with standard large eddy simulations (LESs) in Geurts and Holm (2002, 2003). These numerical tests show various improvements due to the α regularizations over standard subgrid-scale models.

The α model's fluid stability properties have also been discussed in the literature. The α model's effect on elliptical instability was presented in Fabijonas and Holm (2003), where shifts in both the onset and growth rates due to the α-turbulence modification were found. Likewise, the onset of instability shifts to lower wavenumbers for two-layer baroclinic instability (Holm and Wingate 2004, manuscript submitted to *J. Phys. Oceanogr.*). They also showed that the Lagrangian averaging, because it retains important conservation laws, preserves the fundamental stability mechanism found for the unaveraged case, a phenomenon not shared by Eulerian-averaged methods.

In this work the numerical stability of the shallow water α model (SW-α) is investigated. First the α model is reviewed, then its plane wave solutions are presented. Next, section 2 connects the α model to time-implicit numerical methods through the use of the modified equation. Following that, in section 3 an asymptotic estimate of the maximum allowable time step for the

Corresponding author address: B. A. Wingate, Computer and Computational Sciences and Center for Nonlinear Studies, Los Alamos National Laboratory, MS B413, Los Alamos, NM 87545.
E-mail: wingate@lanl.gov

linearized SW-α equations is presented. This result shows that the SW-α time step restriction becomes independent of N, the maximum resolvable wavenumber, as in a time-implicit formulation of the SW equations. In fact, the SW-α model and time-implicit numerical methods share a similar philosophy in that they both lower the frequency of the high wavenumbers to allow a larger maximum allowable time step. This naturally leads to a comparison between them in section 4 for pure gravity waves by Fourier analysis and numerical simulations. Afterward the impact of the α-model formulation on Rossby waves is briefly discussed, (section 5). Section 6 gives a summary of the principal results.

a. Review of the shallow water α model

The Lagrangian-averaged derivation of the α model (Holm et al. 1998) produces equations that are more computable than the NS equations. For example, Foias et al. (2001) show that these equations have a finite dimensional attractor and have proved existence and uniqueness in the strong form for periodic domains, which has not been proved for the NS equations.

Unlike many other averaged versions of the NS equations, the NS-α equations preserve the basic transport structure of the NS equations. For example, they have a Kelvin circulation theorem and conserve energy in an H^1 norm [see Eq. (7)]. In addition, the NS-α equations are a pseudomomentum closure (see Holm 2002) to the generalized Lagrangian mean (GLM) equations of Andrews and McIntyre (1978). The NS-α equations regularize the NS equations through nonlinear dynamics, not through added dissipation.

We restrict ourselves to the SW-α equations, originally derived in Holm (1999), on a β plane,

$$\frac{d}{dt}\mathbf{v} + \nabla\mathbf{u}^{\mathrm{T}}\cdot\mathbf{v} - \mathbf{f}\times\mathbf{u} + \nabla p = \nu\nabla(H\nabla\mathbf{v}), \quad (1)$$

$$\frac{\partial h}{\partial t} + \nabla\cdot(H\mathbf{u}) = 0, \quad (2)$$

where

$$p = gh - \frac{1}{2}|\mathbf{u}|^2 - \frac{\alpha^2}{2}(|\nabla\mathbf{u}|^2), \quad (3)$$

$$\frac{d}{dt} = \frac{\partial}{\partial t} + \mathbf{u}\cdot\nabla, \quad (4)$$

$$H\mathbf{v} = [H - \alpha^2\nabla(H\nabla)]\mathbf{u}. \quad (5)$$

Here $H = h + h_B$ is the total height of the fluid, h_b is the mean depth to the bottom, h is the deviation of the free surface from the mean depth H, f is the Coriolis parameter, and ν the viscosity. There are two velocities in this formulation: $\mathbf{v}$ is interpreted as the Lagrangian mean velocity, while $\mathbf{u}$ is the smoother Eulerian mean velocity. The Eulerian mean velocity advects the Lagrangian mean velocity. The pseudomomentum closure to GLM, Eq. (5), relates these two velocities. In addition there is an extra advection term on the left-hand side of (1). These subtle changes in the nonlinearity, along with the redefined pressure in Eq. (3), cause the large scales to sweep length scales smaller than α. While a thorough examination of this phenomenon is beyond the scope of this work, this sweeping is examined for the linear case and manifests itself in changes to the dispersion characteristics of the linear waves that reduce the frequency of the high wavenumbers. The effect of using the Helmholtz operator to smooth the advecting velocity is not dissipative because with $\nu = 0$ Eqs. (1)–(5) are time reversible.

In deriving these equations the Eulerian mean displacement fluctuation covariance is modeled as $\langle\xi\xi\rangle^{\mathrm{E}} = \alpha^2\mathbf{I}$, which replaces the tensor with a scalar (Holm 1999). This reduces the covariance tensor of the fluctuations to its isotropic homogeneous form. In practice α is the length scale below which the smallest scales are swept, not damped, by the fluid. We restrict ourselves to the case where α is a constant.

With $\nu = 0$, these equations possess the following Kelvin's circulation theorem:

$$\frac{d}{dt}\int_{\gamma(\mathbf{u})}(\mathbf{v} + \mathbf{R})\cdot dx = 0, \quad (6)$$

where $\gamma(\mathbf{u})$ is the fluid loop in the smoothed, Eulerian mean velocity and conserve energy,

$$\frac{1}{2}\frac{d}{dt}\int d^2x[H(\mathbf{u}^2 + \alpha^2|\nabla\mathbf{u}|^2) + gh^2] = 0, \quad (7)$$

and potential vorticity,

$$\frac{d}{dt}\left(\frac{Q_{\mathrm{pv}}}{H}\right) = 0, \quad (8)$$

$$Q_{\mathrm{pv}} = \hat{z}\cdot\mathrm{curl}(\mathbf{v} + \mathbf{R}), \quad (9)$$

where Q_{pv} is the vertical component of the potential vorticity, and $\mathrm{curl}\mathbf{R}(x) = 2\Omega(x) = f(x)$ is the rotation. In the limit as α goes to zero, we recover the shallow water equations.

Domaradzki and Holm (2001) formulate the α model as an LES model written only in terms of the smoothed velocity, $\mathbf{u}$. Numerical experiments replacing the Helmholtz operator, as in Eq. (5), with filtering have been carried out in Geurts and Holm (2002, 2003).

These equations have linear wave solutions similar to those of the SW equations. The two time scales of interest are $\tau_g = L/U$, where L is a typical horizontal length scale and U is a typical velocity scale for gravity waves, and $\tau_r = 1/\beta\lambda_r$ for Rossby waves. The Rossby deformation radius is $\lambda_r = \sqrt{gH_o}/f_o$, and the beta parameter $\beta = \partial_y f$ is the beta-plane approximation. Next the plane wave solutions for gravity waves and Rossby waves are discussed.

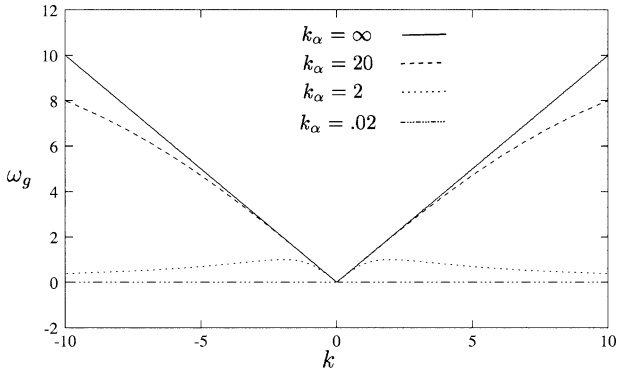

FIG. 1. Nondimensional frequency vs wavenumber for gravity waves. The α model closely approximates the gravity wave frequency for low wavenumbers but reduces the frequency for high wavenumbers. When $k_\alpha = \infty$, it recovers the dispersion relation for SW gravity waves.

b. Plane waves solutions of the α model

1) PURE GRAVITY WAVES

To examine the maximum allowable time step we are principally interested in the fastest waves allowed by the system of equations. For SW these are the pure gravity waves that are unaffected by rotation. To find these waves we set the rotation to zero and assume a flat bottom so that $h_b = H_o$. We then nondimensionalize with time scale τ_g, velocity scale U, length scale L, and height scale H_o and then linearize and rewrite in terms of the divergence ($\delta = u_x + v_y$) and height to obtain

$$\partial_t \delta + \frac{1}{F^2}\nabla^2 h = 0, \tag{10}$$

$$\partial_t h + \overline{\delta} = 0, \tag{11}$$

$$\delta = (1 - \alpha^2\nabla^2)\overline{\delta}, \tag{12}$$

where $F = U/\sqrt{gH_o}$, is the Froude number.

Upon substituting (12) into (10) the system of equations is clearly inherently implicit because of the linear operator, $\alpha^2\nabla^2\partial_t$, acting on $\overline{\delta}$. So, for nonzero α these equations resemble a modified form of time-implicit differencing, which is discussed more in section 2.

Substituting in the Fourier modes for the dependent variables with nondimensional wavenumbers $(k, l) = L(k', l')$ and $\omega = L\omega'/U$ (where the primes denote the dimensional quantities), we find the nondimensional dispersion relation to be

$$\omega_g^2 = \frac{k_h^2}{F^2(1 + \alpha^2 k_h^2)} \quad \text{or}$$

$$\omega_g^2 = \frac{k_h^2}{F^2[1 + (k_h/k_\alpha)^2]}, \tag{13}$$

where $k_h^2 = k^2 + l^2$ and $k_\alpha = 1/\alpha$ is the α wavenumber. This dispersion relation is shown in Fig. 1. The solid line is the case for $\alpha = 0$, the SW equations. The other three lines show the effect of increasing α (reducing k_α). For large values of k_α the frequency of the low wavenumbers is unchanged. As k_α decreases, the bandwidth of waves that mimic the frequency of the SW gravity waves decreases. Eventually the frequency for all wavenumbers is zero. The effect of incorporating the small scales on the large through the Lagrangian averaged α model is to slow down the frequency of the high wavenumbers.

2) ROSSBY WAVES

Nondimensionalizing Eqs. (1)–(2) using the Rossby wave time scale τ_r, instead of the gravity wave time scale τ_g, and keeping only terms $O(\mathrm{Ro})$ and higher,

$$(\partial_t + u_1\partial_x + u_2\partial_y)(R_o\zeta + \beta'' y) + \overline{\delta} = 0, \tag{14}$$

$$\mathrm{Ro}(\partial_t + u_1\partial_x + u_2\partial_y)h + B^2\overline{\delta} = 0, \tag{15}$$

$$\psi = (1 - \alpha^2\nabla^2)\overline{\psi}, \qquad \zeta = \nabla^2\psi,$$
$$u_1 = -\overline{\psi}_y, \qquad u_2 = \overline{\psi}_x, \qquad h = \overline{\psi}, \tag{16}$$

where $\mathrm{Ro} = U/(f_o L)$, $B^2 = \lambda_r^2/L^2$, and $\beta'' = \beta L/f_o$. Writing this in terms of the vorticity $\zeta = v_{2x} - v_{1y}$, and the divergence $\overline{\delta} = u_{1y} + u_{2y}$, rescaling to the τ_g time scale (to be consistent with the last section) and linearizing, we obtain

$$\partial_t\nabla^2(1 - \alpha^2\nabla^2)\overline{\psi} + \beta'\overline{\psi}_x - \frac{1}{B^2}\partial_t\overline{\psi} = 0, \tag{17}$$

where $\beta' = \beta L^2/U$. Then the α-model dispersion relation is

$$\omega_r = \frac{-k\beta'}{k_h^2(1 + \alpha^2 k_h^2) + 1/B^2} \quad \text{or}$$

$$\omega_r = \frac{-k\beta'}{k_h^2[1 + (k_h^2/k_\alpha)^2] + k_r^2}. \tag{18}$$

As in the case of the gravity waves, α has the effect of slowing down the frequency of the high wavenumbers. Figure 2 shows this effect for three different cases. The solid line is the case when $\alpha = 0$ and shows the usual maximum frequency at the Rossby deformation wavenumber, $k_r = 1/B^2$. The dashed line is the case when $k_\alpha \gg k_r$. The effect is twofold. First, the α model shifts the maximum of the curve to a lower wavenumber; second, most of the wavenumbers to the right of the maximum are close to those of the unaveraged equations, while those to the left have lower frequencies. If we define the deformation wavenumber as the place where the Rossby wave frequency is a maximum, then the α modification defines a new deformation wavenumber, k_r^α, that depends on both α and k_r. This new deformation wavenumber is

$$k_r^\alpha = -\frac{1}{6}\sqrt{-6k_\alpha^2 - 6k_\alpha\sqrt{k_\alpha^2 + 12k_r^2}}$$
$$\forall \quad k_\alpha, k_r < 0. \tag{19}$$

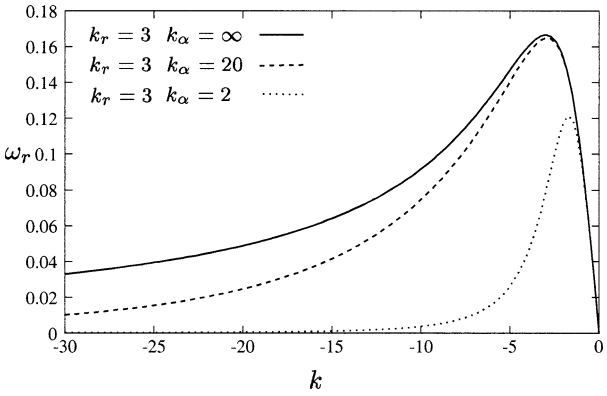

FIG. 2. Nondimensional frequency vs wavenumber for Rossby waves for $\beta' = 1$. The solid line, $k_\alpha = \infty$ shows the usual maximum at the Rossby deformation radius k_r. The dashed line, $k_\alpha \gg k_r$, reveals two effects. First, the α model shifts the maximum to the lower wavenumber. Second, most of the wavenumbers to the right of the maximum are faithfully approximated, while those to the left have lower frequencies. The dotted line shows the case when $k_\alpha < k_r$. The maximum is substantially shifted to the right, and the frequency at high wavenumbers is zero. If the Rossby deformation wavenumber is located where the frequency is the maximum then one key effect of the model is to define a new deformation wavenumber, $k_r^\alpha < k_r$ [Eq. (19)].

Therefore, the Rossby deformation radius for equations that describe the slow time dynamics through the α model occurs at a lower wavenumber than for the SW equations that describe the unaveraged, instantaneous dynamics.

2. Connection to implicit time differencing

To understand the impact of using Lagrangian averaging to model the effects of small scales on the large, its linear analysis is compared to that of implicit-in-time numerical methods.

The α model is derived from Hamilton's principle through Lagrangian averaging and represents the mean, or slow-time dynamics of the fluid. It changes the nonlinearity considerably, making a detailed analysis difficult. But, as shown above, it makes interesting changes even in the linear theory. In particular, the α model lowers the frequency of the waves at high wavenumbers, because the high-wavenumber motions are accounted for in the large-scale motion through the Lagrangian averaging. This linear behavior is similar to implicit time differencing in partial differential equations. They both result in unconditional numerical stability through modifications to the linear dispersion and damping properties of the high-frequency waves that cannot be resolved by a given time step.

In this section I elaborate on this connection between the α model and implicit numerical time differencing through the use of the modified equation (see Hirt 1968; Warming and Hyett 1974). The modified equation is derived by expanding each term of a difference scheme in a Taylor series and then eliminating time derivatives higher than some order by algebraic manipulation. This equation represents the actual partial differential equation solved by the given numerical method.

At the end of this section I show a semi-implicit numerical discretization of the linear gravity waves that mirrors the explicit discretization of the α model's linear waves. This connection is helpful in understanding the linear behavior of the α model, but I am in no way suggesting this discretization should replace others used in the literature because of the impact of the nonlinearity, which is beyond the scope of this work.

We begin by examining the backward-in-time discretization of Eqs. (10)–(12). Since we want to compare the implicit time difference of the SW equations to the α model, we set $\alpha = 0$,

$$\delta^{m+1} - \delta^m + \frac{\Delta t}{F^2}\nabla^2 h^{m+1} = 0, \tag{20}$$

$$h^{m+1} - h^m + \Delta t \delta^{m+1} = 0. \tag{21}$$

Above, the superscript indicates time level, m is at time level t, and $m + 1$ is at time level $t + \Delta t$. We next apply a Taylor expansion to the terms about time level $m + 1/2$,

$$\delta^{m+1} = \delta^{m+1/2} + \frac{\Delta t}{2}\left(\frac{\partial \delta}{\partial t}\right)^{m+1/2},$$

$$\delta^{m} = \delta^{m+1/2} - \frac{\Delta t}{2}\left(\frac{\partial \delta}{\partial t}\right)^{m+1/2},$$

$$h^{m+1} = h^{m+1/2} + \frac{\Delta t}{2}\left(\frac{\partial h}{\partial t}\right)^{m+1/2},$$

$$h^{m} = h^{m+1/2} - \frac{\Delta t}{2}\left(\frac{\partial h}{\partial t}\right)^{m+1/2},$$

and substitute these into Eqs. (20)–(21) while dropping terms higher order than Δt^2,

$$\partial_t \delta^{m+1/2} + \frac{1}{F^2}\nabla^2\left(h^{m+1/2} + \frac{\Delta t}{2}\partial_t h^{m+1/2}\right) = 0, \tag{22}$$

$$\partial_t h^{m+1/2} + \delta^{m+1/2} + \frac{\Delta t}{2}\partial_t \delta^{m+1/2} = 0. \tag{23}$$

Algebraic manipulation gives

$$\left(1 - \frac{\Delta t^2}{4F^2}\nabla^2\right)\partial_t \delta + \frac{1}{F^2}\nabla^2 h = \frac{\Delta t}{2F^2}\nabla^2 \delta, \tag{24}$$

$$\left(1 - \frac{\Delta t^2}{4F^2}\nabla^2\right)\partial_t h + \delta = \frac{\Delta t}{2F^2}\nabla^2 h. \tag{25}$$

When $\Delta t = 0$ Eqs. (24) and (25) become the SW equations for gravity waves given in Eqs. (10)–(12) with $\alpha = 0$. When $\Delta t \neq 0$ the additional terms on the left-hand side represent changes in the dispersion of the waves

while the terms on the right-hand side represent diffusion.

Any number of choices in the time differencing will result in different modified equations. Any form of implicit time differencing results in dispersion truncation error terms that resemble those on the left-hand sides of Eqs. (24)–(25). It is these terms that result in the dispersion relations such as (13) that yield numerical time stability. To obtain a modified equation similar to that of the α model, choose

$$\delta^{m+1} - \delta^m + \frac{\Delta t}{F^2}\nabla^2 h^{m+1} = 0, \tag{26}$$

$$h^{m+1} - h^m + \Delta t \delta^{m+1/2} = 0. \tag{27}$$

Applying a Taylor expansion to the term about $m + 1/2$ and retaining up to terms of order Δt^2, we arrive at

$$\left(1 - \frac{\Delta t^2}{4F^2}\nabla^2\right)\partial_t \delta + \frac{1}{F^2}\nabla^2 h = \frac{\Delta t}{2F^2}\nabla^2 \delta, \tag{28}$$

$$\partial_t h + \delta = 0. \tag{29}$$

The only difference between the above equations and Eqs. (10)–(12) is the additional diffusion term on the right-hand side of Eq. (28). From these equations we see the α model is ''born'' implicit (Caramana 1991) in that α models obtain terms of the form $\alpha^2\nabla^2\partial_t$ that when discretized lead to spatially coupled systems. The connection between the parameter α and the time step Δt is seen simply as $\alpha^2 = \Delta t^2/4F^2$. Therefore, to lowest order, choosing an α for the α model is similar to choosing a time step in an implicit method. This implies in a generic sense that for the linearized equations there is a similar type of spatial averaging in both cases.

This connection allows us to understand the linear behavior of the α model in terms of familiar implicit-in-time numerical discretizations. But the α-model equations describe the Lagrangian mean motion, while the implicit-in-time method is simply a numerical discretization of the unaveraged motion of the SW equations. Equations (28)–(29) are not necessarily a good numerical discretization for the unaveraged, nonlinear SW equations.

3. Estimate for the maximum allowable time step

An estimate for the maximum allowable time step is obtained by examining the asymptotic stability properties of the fastest-moving waves of the system. For the SW equations these are the highest-wavenumber gravity waves supported by the numerical mesh.

We discretize in time and apply the Fourier method in space. Then, for some vector $\mathbf{U}$, we consider

$$\frac{d\mathbf{U}}{dt} = \mathbf{L}\mathbf{U}, \tag{30}$$

where $\mathbf{L}$ is the matrix resulting from the Fourier decomposition of Eqs. (10)–(12). The time-stepping method is asymptotically stable if for a sufficiently small $\Delta t > 0$ the product of Δt and every eigenvalue of $\mathbf{L}$ denoted by ω_g, lies in the domain of absolute stability,

$$\omega_g \Delta t \le C. \tag{31}$$

If Eq. (31) is true, then some spatial norm of the numerical solution at some fixed time, t^n, is bounded for $t \to \infty$. Parameter C, the maximum for the domain of stability is well known for many method-of-lines approaches (see Canuto et al. 1988). For example, for the third-order Adams–Bashforth method, $C = 0.723$.

We next denote the highest wavenumber as $k = l = N$ and substitute into ω_g, given by Eq. (13) and then substitute that expression into Eq. (31) and solve for Δt:

$$\Delta t \le \frac{C}{\omega_g}, \tag{32}$$

$$\le \frac{CF\sqrt{(1 + 2\alpha^2 N^2)}}{\sqrt{2N^2}}, \tag{33}$$

and as $N \to \infty$,

$$\Delta t \le CF\alpha. \tag{34}$$

This shows that for fixed α, as the number of modes in the solution increases, the maximum allowable time step for the α model becomes independent of N. Finally, we compare Eq. (34) to that for the SW equations,

$$\Delta t \le \frac{CF}{\sqrt{2}N}. \tag{35}$$

The maximum allowable time step for the SW equations decreases linearly with N, the highest wavenumber, while for the α model it becomes independent of N.

Time-implicit numerical methods also slow down the frequency of the highest wavenumbers. In fact, the α model and time-implicit numerical methods share the same philosophy in that both methods modify the frequency of the high wavenumbers in order to attain higher maximum allowable time steps. The similarity and difference will become clearer in the next section.

4. Pure gravity waves

In section 2 a connection was established between the α model and implicit numerical schemes. Through two very different mechanisms (one dynamical, one numerical), they slow down the frequency of the high wavenumbers and can therefore take a time step beyond the explicit time step limit of the SW equations.

The principal aim of this section is to study the numerical differences between an explicit formulation of the SW-α model to the familiar time-implicit method of Dukowicz and Smith (1994, hereafter DS94). We begin with a Fourier analysis of both to compare amplitude and dispersion errors and then compare numerical simulations.

a. Fourier analysis

Define $\lambda = e^{-i\omega\Delta t}$ or $\lambda = |\lambda| e^{-i\,\mathrm{Re}(\omega\Delta t)}$, where ω can be either the dispersion relation for the Rossby or gravity waves, $\mathrm{Re}(\omega\Delta t)$ is the phase per unit time step, and $|\lambda|$ is the amplification factor.

1) ADAMS–BASHFORTH DISCRETIZATION OF SW-α

First we discretize Eqs. (10)–(12) with a common time-stepping scheme, the third-order Adams–Bashforth method (AB3), and compare the numerical phase speed and amplitude with their analytical counterparts in Eq. (13):

$$\delta^{n+1} - \delta^n + \frac{\Delta t}{F^2}\left(\frac{23}{12}\nabla^2 h^n - \frac{16}{12}\nabla^2 h^{n-1} + \frac{5}{12}\nabla^2 h^{n-2}\right) = 0, \tag{36}$$

$$h^{n+1} - h^n + \Delta t\left(\frac{23}{12}\overline{\delta}^n - \frac{16}{12}\overline{\delta}^{n-1} + \frac{5}{12}\overline{\delta}^{n-2}\right) = 0, \tag{37}$$

$$\delta^n = (1 - \alpha^2\nabla^2)\overline{\delta}^n. \tag{38}$$

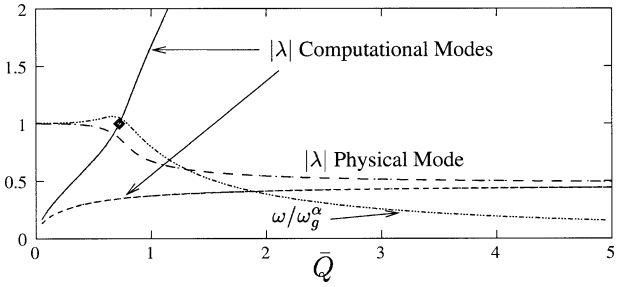

FIG. 3. Damping factor and frequency vs $\overline{Q}$ for AB3. This is the usual stability diagram for an AB3 discretization of SW gravity waves with the exception that the CFL parameter is $\overline{Q}$ instead of Q, where $Q^2 = dt^2k_h^2$, and the two are related by Eq. (40).

Using the Fourier method for the spatial discretization, we then substitute $\delta = \lambda\hat{\delta}\exp[i(kx + ly)]$ and $h = \lambda\hat{h}\exp[i(kx + ly)]$ into Eqs. (36)–(38), where $k_h^2 = k^2 + l^2$ and take the determinant and set it equal to zero to produce the characteristic equation:

$$(\lambda - 1)^2\lambda^4 + \frac{\Delta t^2k_h^2}{F^2(1 + \alpha^2k_h^2)}\left(\frac{23}{12}\lambda^2 - \frac{16}{12}\lambda + \frac{5}{12}\right)^2. \tag{39}$$

When $\alpha = 0$, we recover the characteristic polynomial for the shallow water equations. Denote

$$\overline{Q}^2 = \frac{\Delta t^2k_h^2}{F^2(1 + \alpha^2k_h^2)} = \frac{Q^2}{(1 + \alpha^2k_h^2)}. \tag{40}$$

Figure 3 shows the numerically computed amplification factor and phase error, versus $\overline{Q}$. This is the usual stability result for an AB3 discretization of SW gravity waves except that $\overline{Q}$ represents the Courant–Friedrichs–Lewy (CFL) number, instead of Q, where $Q^2 = \Delta t^2k_h^2$. This plot shows that for numerical stability,

$$\overline{Q} \le C, \tag{41}$$

where the explicit stability limit is marked on the figure with a diamond. Substitute Eq. (40) into (41),

$$\sqrt{\frac{2\Delta t^2k_h^2}{F^2(1 + 2\alpha^2k_h^2)}} \le C. \tag{42}$$

We parallel the analysis of section 3 by substituting the highest wavenumber ($k_h^2 = 2N^2$) into Eq. (42), and taking the limit as $N \to \infty$,

$$\frac{\Delta t}{F\alpha} \le C. \tag{43}$$

Finally, we solve for Δt,

$$\Delta t \le CF\alpha. \tag{44}$$

This result is the same as Eq. (34). That is, the maximum allowable time step becomes independent of N.

Exploring the relationship between $\overline{Q}$, the α model's CFL parameter, and Q, the usual CFL parameter, we plot Eq. (40) in Fig. 4. When $k_\alpha = \infty$ ($\alpha = 0$), the CFL parameters are identical. As k_α increases, the CFL parameter for the α model decreases relative to the SW CFL parameter, stabilizing the method. Though not plotted here, when $k_\alpha = 0$ ($\alpha = \infty$), $\overline{Q}$ is zero for all frequencies and wavenumbers, making the SW-α equations unconditionally stable.

Figure 5 shows the maximum allowable time step for $F = 1$, computed by solving Eq. (42) for Δt:

$$\Delta t < \frac{CF\sqrt{1 + \alpha^2k_h^2}}{k_h}. \tag{45}$$

For $\alpha = 0$ we find the $1/k$ behavior we expect. As a increases, the maximum allowable time step asymptotes to $CF\alpha$ in k and becomes independent of wavenumber. The larger α, the larger the maximum allowable time step.

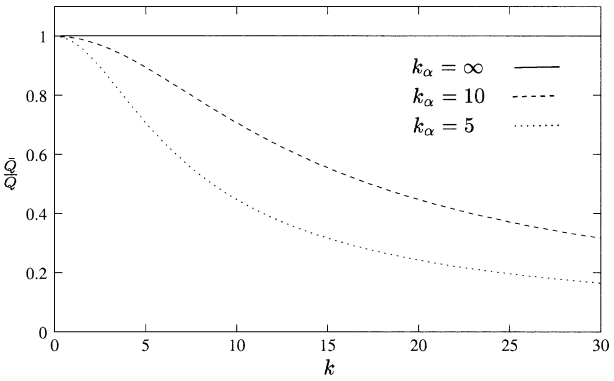

FIG. 4. This figure shows how $\overline{Q}/Q$ changes for a given k_α and wavenumber where $\overline{Q}$ is the modified CFL parameter for the α model, and Q is the usual CFL parameter. The solid line, for $k_\alpha = \infty$ ($\alpha = 0$), shows that the CFL parameter for the SW-α model is the same as for the SW equations. As k_α decreases the CFL parameter for the α model decreases relative to the SW CFL parameter stabilizing the method.

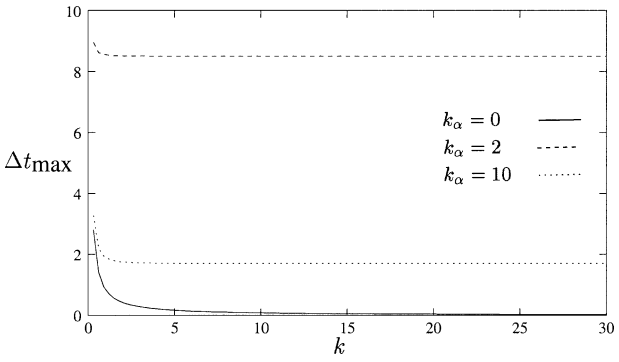

FIG. 5. Maximum allowable time step of Eq. (45) vs wavenumber. For $\alpha = 0$ we find the $1/k$ behavior we expect for SW gravity waves. As α increases the maximum allowable time step asymptotes to $C\alpha$ in k and becomes independent of wavenumber.

2) IMPLICIT FREE SURFACE DISCRETIZATION OF SW

In this section we compare the α model of the previous section to the method of DS94 because it is the method employed in the widely used Parallel Ocean Program (POP) ocean model (Dukowicz et al. 1993). In their method, DS94 use the time-implicit method for the 2D barotropic equations to advance the fastest-moving waves, while using a more accurate explicit numerical scheme to advance the slow, 3D baroclinic modes. We focus only on their time-implicit method for the 2D barotropic equations, which are very similar to the SW equations studied in this paper. We repeat the DS94 discretization and analysis here for completeness:

$$\delta^{n+1} - \delta^{n-1} + \frac{2\Delta t}{F^2}\nabla^2 h^\mu = 0, \tag{46}$$

$$h^{n+1} - h^n + \Delta t\delta^\theta = 0, \tag{47}$$

where,

$$\chi^\mu = \mu\chi^{n+1} + (1 - \mu - \gamma)\chi^n + \gamma\chi^{n-1}, \tag{48}$$

$$\chi^\theta = \theta\chi^{n+1} + (1 - \theta)\chi^n, \tag{49}$$

where χ can be either h, δ, or in later sections ψ. Substituting $\delta = \lambda e^{ik_h x}\hat{\delta}$, $h = \lambda e^{ik_h x}\hat{h}$, into the above, we obtain the characteristic polynomial

$$(\lambda^2 - 1)(\lambda - 1) + \frac{2Q^2}{F^2}[\mu\lambda^2 + (1 - \mu - \gamma)\lambda + \gamma]$$

$$\times (\theta\lambda + 1 - \theta) = 0. \tag{50}$$

Figure 6 shows numerically computed amplification factors and dispersion errors versus Q, where $Q^2 = \Delta t^2 k_h^2$, for their near-optimal parameter choices, $\mu = \gamma = 1/3$, $\theta = 1$:

$$Q^2 = \Delta t^2 k_h^2. \tag{51}$$

Comparing Figs. 3 and 6, we first see that the α model does not appear to be unconditionally stable, unlike DS94. But it can be made so by increasing α, thus reducing $\overline{Q}$, as shown in Fig. 5. As α is increased, the time step increases, and the solution to the α model, the modeled Lagrangian mean solution, incorporates more of the small scales on the large, moving further away from the instantaneous solutions of the SW equations. In the time-implicit numerical method a similar effect happens—the larger the time step, the further the solutions are from the instantaneous SW solutions.

b. Numerical test case

In the case of SW-α the time step gain originates from the Lagrangian mean solutions of the partial differential equation (PDE). That is, the small scales have been incorporated into those of the large in the solutions to SW-α, which subsequently slows down the frequency at the high wavenumbers. This allows a larger time step to be taken. The method of DS94 also allows a time step beyond the explicit limit through the implicit numerical formulation of the unaveraged SW equations. I

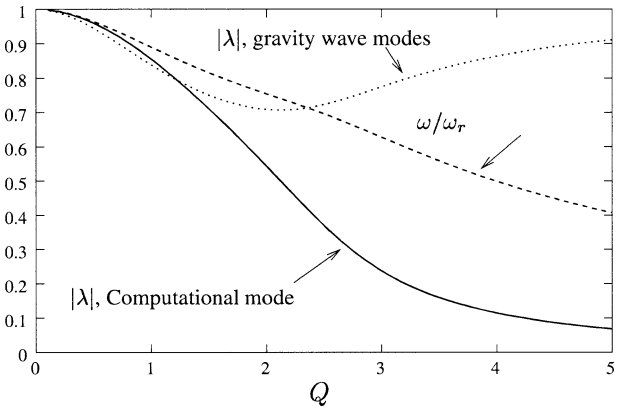

FIG. 6. Amplification factor, denoted by $|\lambda|$, and phase error, denoted by ω/ω_r, vs Q, the CFL parameter, for the near-optimal parameter choices for the semi-implicit method of DS94.

wish to further examine the differences in these two methods. Therefore, this section focuses on the comparison of a single, simple test case, described below. Both the α-model numerical solutions and the DS94 solutions to the exact solutions of the SW equations are compared to examine their behavior relative to the unaveraged SW equations.

To draw out the effects of SW-α and DS94 in different wavenumber parts of the solution I focus on a test case comprised of a superposition of high- and low-wavenumber waves. Again, this investigation is restricted to the linear equations for pure gravity waves (no rotation).

Rewrite Eqs. (10)–(12) as

$$\partial_t v_1 + \frac{1}{F^2}\partial_x h = 0, \tag{52}$$

$$\partial_t v_2 + \frac{1}{F^2}\partial_y h = 0, \tag{53}$$

$$\partial_t h + \partial_x u_1 + \partial_y u_2 = 0, \tag{54}$$

$$\mathbf{v} = (1 - \alpha^2\nabla^2)\mathbf{u}. \tag{55}$$

An analytical solution to these equations is

$$u_1 = \frac{k}{F^2\omega A(k, l, \alpha)} \cos(xk - \omega t) \cos(yl),$$

$$v_1 = A(k, l, \alpha)u_1 \tag{56}$$

$$u_2 = -\frac{l}{F^2\omega A(k, l, \alpha)} \sin(xk - \omega t) \sin(yl),$$

$$v_2 = A(k, l, \alpha)u_2 \tag{57}$$

$$h = \cos(xk - \omega t) \cos(yl) \quad \text{and}$$

$$A(k, l, \alpha) = [1 + \alpha^2(k^2 + l^2)]. \tag{58}$$

We superimpose a $k = l = 20$ solution with a $k = l = 3$ solution:

$$u_1^t = a_3 u_1|_{k=l=3} + a_{20} u_1|_{k=l=20}, \tag{59}$$

$$u_2^t = b_3 u_2|_{k=l=3} + b_{20} u_2|_{k=l=20}, \tag{60}$$

$$h^t = c_3 h|_{k=l=3} + c_{20} h|_{k=l=20}, \tag{61}$$

where the coefficients are chosen to be $a_3 = b_3 = c_3 = 0.9$ and $a_{20} = b_{20} = c_{20} = 0.1$. Figure 7 depicts a one-dimensional slice at $y = 1.521\,708\,94$. We integrate the α-model and DS94 in time until $t = 4.44$, the time to propagate a wavenumber-1 solution one period.

1) Results for the test case from Fourier analysis

Now we evaluate at the L_2 norm of the error for the high and low frequencies of the test case.

We define the L_2 norm as:

$$\|w\|_{L^2} = \left(\frac{1}{4\pi^2}\int_0^{2\pi}\int_0^{2\pi} |w|^2\, dx\, dy\right)^{1/2}, \tag{62}$$

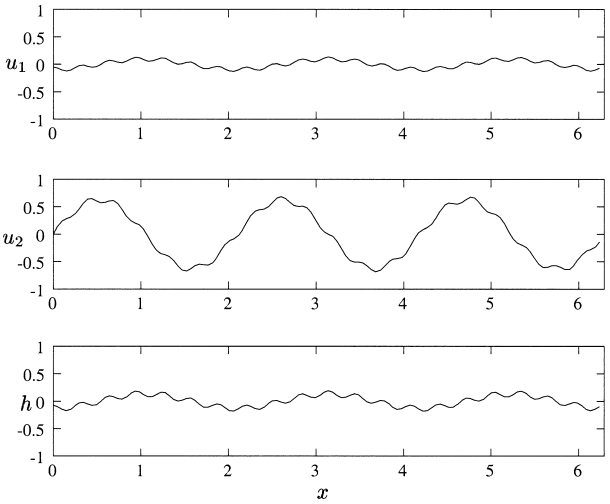

FIG. 7. Test case solution at $t = 0$ at $y = 1.521\,708\,94$.

where w is a function defined on $(x, y) \in (0 \ldots 2\pi, 0 \ldots 2\pi)$. We choose this function to be the error between the exact solution and the computed solution, $w = h_{\text{exact}} - h_{\text{computed}}$. Recalling that $h = \hat{h}|\lambda|^n e^{-i\omega_r^c n\Delta t} e^{ik_h x}$ from our analysis in section 3 we can compute the L_2 norm of the error for both DS94 and the α model by

$$\|w\|_{L^2} = \left(\frac{1}{4\pi^2}\int_0^{2\pi}\int_0^{2\pi} |e^{-i\omega_g t} - |\lambda|^n e^{-i\omega_g^c t}|^2\, dx\, dy\right)^{1/2}. \tag{63}$$

These errors are a function of wavenumber and time. We plot the L_2 errors in Fig. 8. Figure 8a shows the L_2 error for both wavenumbers. For the high-wavenumber solution, both DS94 and the α model make the same error relative to the instantaneous SW equations by the time $t = 4.44$. The error for the low wavenumber, 3, is less in the case of the α model by about a factor of 2.

Now define an amplitude and phase L_2 error as

$$\|w\|_{L^2}^{\text{amp}} = \left[\frac{1}{4\pi^2}\int_0^{2\pi}\int_0^{2\pi} (1 - |\lambda|^n)^2\, dx\, dy\right]^{1/2}, \tag{64}$$

$$\|w\|_{L^2}^{\text{phase}} = \left(\frac{1}{4\pi^2}\int_0^{2\pi}\int_0^{2\pi} |e^{-i\omega_g t} - e^{-i\omega_g^c t}|^2\, dx\, dy\right)^{1/2}, \tag{65}$$

where ω_g is Eq. (13), and $|\lambda|$ and ω_g^c are computed numerically using either Eq. (39) in the case of the α model or Eq. (50) in the case of DS94.

Figure 8b shows the amplitude L_2 error, $\|\omega\|_{L^2}^{\text{amp}}$ versus time. We see that both DS94 and the α model make the maximum possible amplitude error for the highest wavenumber. However, for the lowest wave number the α model makes almost no amplitude error, while DS94 makes some amplitude error from its damping. Furthermore, Fig. 8c shows once again that both the α

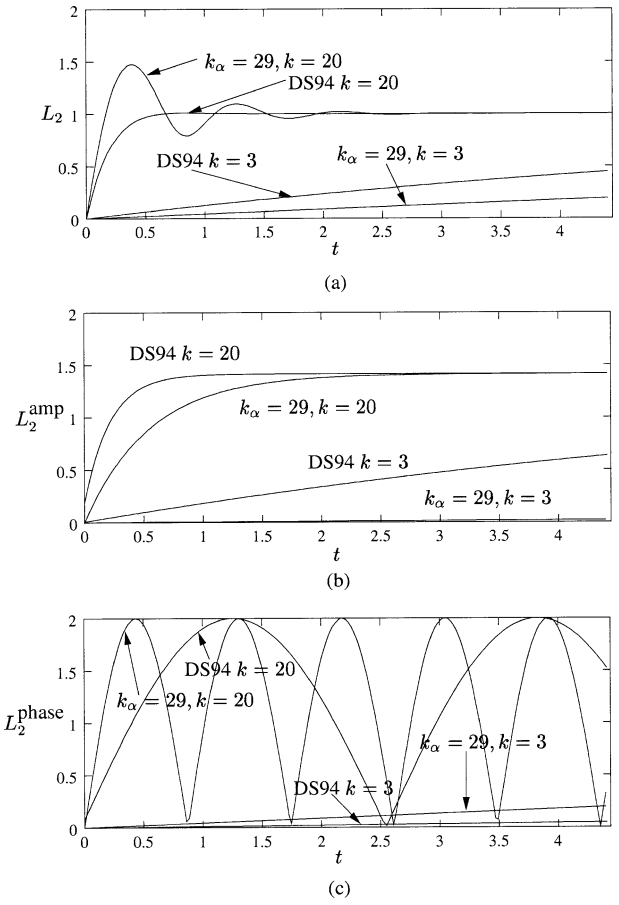

FIG. 8. (a) The L_2 errors described by Eq. (63); (b) $\|\omega\|_{L^2}^{\text{amp}}$; and (c) $\|\omega\|_{L^2}^{\text{phase}}$, where ω_g is Eq. (13), and $|\lambda|$ and ω_g^c are computed numerically using either Eq. (39) in the case of the α model or Eq. (50) in the case of DS94.

model and DS94 make high errors for the high-wavenumber solution. For the low wavenumber, the DS94 phase error is less than that of the α model.

2) RESULTS FOR THE TEST CASE FROM NUMERICAL SIMULATIONS

In this section numerical simulations of the test case are run at three different values of the time step, both for DS94 and for the α model. In all three cases for the α model the largest k_α that gives a stable solution is chosen. Figure 9 shows $\overline{Q}$, the stability parameter for AB3 as a function of α for all three time steps, for the two wavenumbers used in the test case. The solid line across the top of the graph is the stability limit for AB3. When $\alpha = 0$, the method is stable for $\Delta t = 0.01$ and $\Delta t = 0.001$. For the largest time step and highest wavenumber the CFL parameter exceeds the explicit limit. Also, one observes that $\overline{Q}$ asymptotes to a constant as α is increased, confirmation of the stability limit given in section 3. For a stable solution, choose α to be the

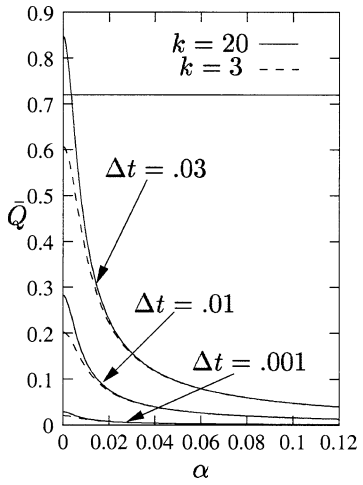

FIG. 9. Parameter $\overline{Q}$ as a function of α for three different time steps and two different wavenumbers, one high frequency (20), the other low (3). The stability limit for AB3 is drawn as a straight line. For the largest time step and highest wavenumber the CFL parameter exceeds the explicit limit.

smallest value that gives the desired value of $\overline{Q}$. The values chosen for the test case are shown in Table 1.

Figure 10 shows the final solution for DS94 and the α model for three different time steps. The top-left panel is for $\Delta t = 0.001$. The α model with $k_\alpha = 1000$ is indistinguishable from the analytical solution for $\alpha = 0$. DS94's damping is already affecting the variability of the solution, lowering the amplitude of the high-frequency oscillations. The top-right panel shows the case where $\Delta t = 0.01$. At this time step the high-frequency part of the solution is gone for DS94, leaving the low frequency intact. The α model with $k_\alpha = 125$ is preserving some of the high-frequency variability. Finally the bottom panel shows the case for $\Delta t = 0.03$. Both DS94 and the α model ($k_\alpha = 29$) have damped the high frequencies. The difference is that DS94 has also damped the low-frequency part of the solution while the α model has preserved some of the amplitude, but has introduced more phase error.

Figure 11 shows the L_2 norm of the error for the test case. The solid lines are the L_2 error for the α model, while the dots are for DS94. For the smallest time step of the test problem, $\Delta t = 0.001$, the α model's error is very small. DS94's error increases over the period of the calculation. As we increase the time step to $\Delta t = 0.01$, the L_2 norm of the error between the DS94 and the α model is about the same. Finally, for the largest time step, $\Delta t = 0.03$, which is beyond the explicit stability limit, we see the L_2 norm of the α model is, at first, very large, and oscillates, eventually asymptoting to roughly the same error as DS94 with the smaller time step of $\Delta t = 0.01$. For the same time step the error for DS94 is larger.

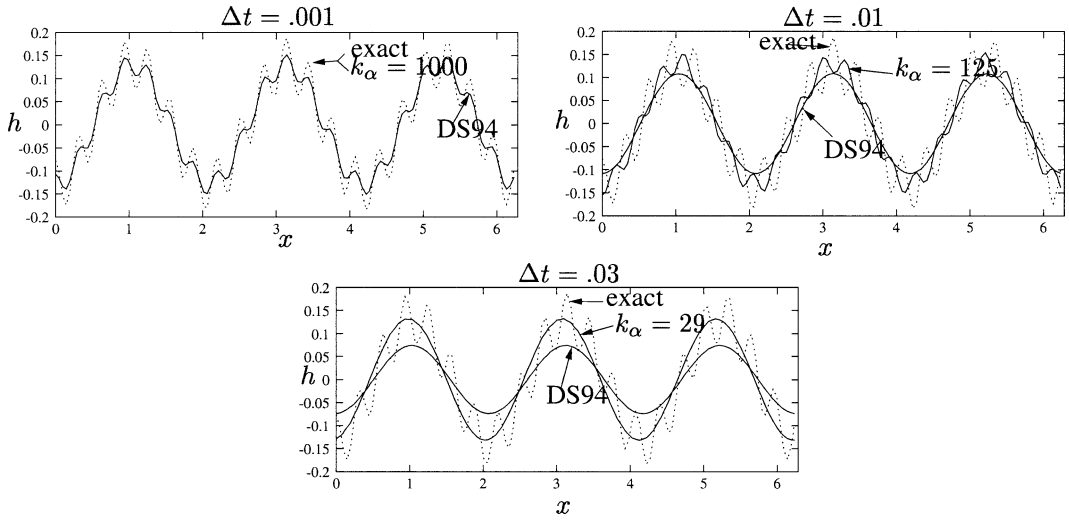

FIG. 10. The α model and DS94 at $t = 4.44$ compared with the exact solution for three different time steps. (top left) The case for $\Delta t = 0.001$. The α model with $k_\alpha = 1000$ is indistinguishable from the analytical solution for $\alpha = 0$. DS94's damping is already affecting the variability of the solution, lowering the amplitude of the high-frequency oscillations. (top right) The case where $\Delta t = 0.01$. At this time step the high-frequency part of the solution is gone for DS94, leaving the low frequency intact. The α model with $k_\alpha = 125$ is preserving some of the high-frequency variability. (bottom) The case for $\Delta t = 0.03$. Both DS94 and the α model ($k_\alpha = 29$) have damped the high frequencies. The difference is that DS94 has also damped the low-frequency part of the solution while the α model has preserved some of the amplitude but has introduced more phase error.

5. Rossby waves

This section investigates the effect of taking a larger time step on Rossby waves. In the semi-implicit method of DS94, this subject is pursued to show that at large time steps the Rossby waves are unaffected. In the case of the α model, taking a large time step corresponds to Lagrangian averaging over a longer time interval. This means more of the smaller scales are incorporated into the large. Here the Fourier analysis of an explicit discretization of the α model is shown and compared to the implicit numerical scheme applied to the unmodeled equations.

a. Adams–Bashforth

The same procedure as in section 4 is followed and Eqs. (14)–(16) are discretized in time using AB3 and the Fourier spectral method in space. Then the Fourier analysis is applied to the discrete equations to find the characteristic polynomial:

$$\nabla^2\psi^{n+1} - \nabla^2\psi^n + \Delta t(\beta'\overline{\psi}_x^{\zeta} + \overline{\delta}^{\zeta}) = 0, \quad (66)$$

$$\overline{\psi}^{n+1} - \overline{\psi}^n + \Delta t B^2\overline{\delta}^{\zeta} = 0, \quad (67)$$

TABLE 1. The values of k_α used in the test problem for the three time steps.

Δt	k_α
0.001	1000
0.01	125
0.03	29

$$\phi^{\zeta} = \frac{23}{12}\phi^n - \frac{16}{12}\phi^{n-1} + \frac{5}{12}\phi^{n-2}. \quad (68)$$

Substituting $\delta = \lambda e^{kx+ly}\hat{\delta}$, $\psi = \lambda e^{kx+ly}\hat{\psi}$,

$$\lambda^2(\lambda - 1)[B^2k_h^2(1 + \alpha^2k_h^2) + 1] - i\Delta tF(\lambda)B^2\beta' k = 0, \quad (69)$$

where

$$F(\lambda) = \frac{23}{12}\lambda^2 - \frac{16}{12}\lambda + \frac{5}{12}.$$

This can be written as

$$\lambda^2(\lambda - 1)\left(k_h^2 + \frac{k_r^2}{1 + k_h^2/k_\alpha^2}\right) - i\frac{\Delta t\beta' kF(\lambda)}{1 + k_h^2/k_\alpha^2} = 0, \quad (70)$$

where

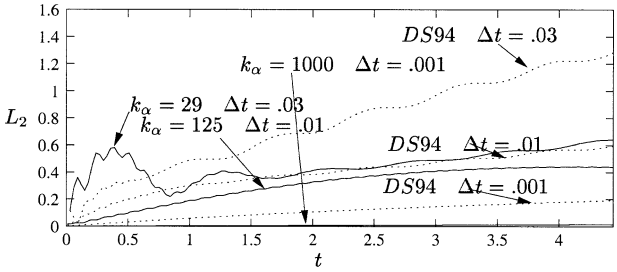

FIG. 11. The L_2 error for DS94 and the α model as a function of time for three different time steps.

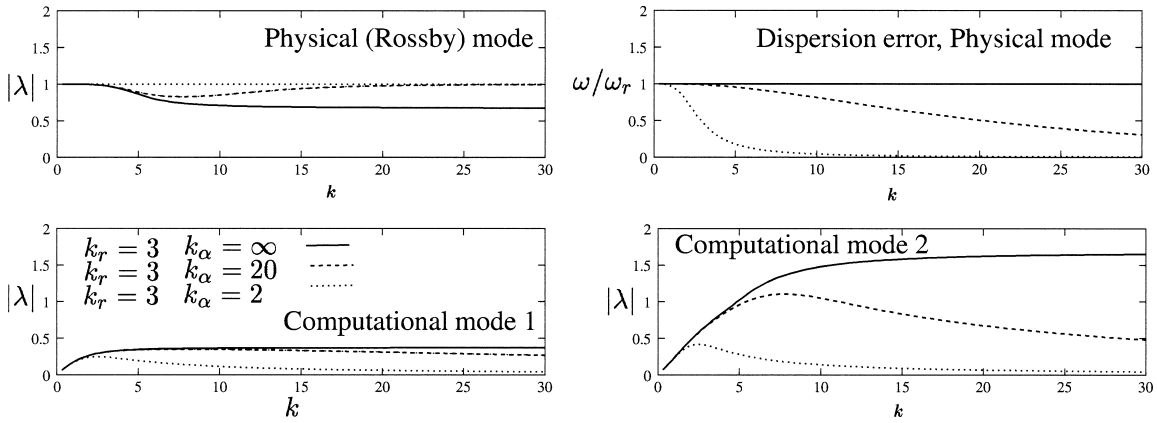

FIG. 12. Numerically computed amplitudes and phase speed errors for the SW-α equations for $\beta' = 1$ and $k_r = 3$, where k_r is the Rossby deformation radius wavenumber. The characteristic equation has three roots, two computational modes, and one physical mode. Computational mode 1 is alway stable. The solid line is for $k_\alpha = \infty$ ($\alpha = 0$), the dashed line represents $k_\alpha = 20$, and the dotted line represents $k_\alpha = 2$. Computational mode 2 is more significantly affected by α. As we decrease the α wavenumber the solution becomes unconditionally stable. The amplitude error in the physical mode asymptotes to zero. The phase speed error, for the lowest k_α is significant, even for small k. Even for large values of α, where the dispersion error is larger, the amplitude of the Rossby waves is reasonably approximated.

$$F(\lambda) = \frac{23}{12}\lambda^2 - \frac{16}{12}\lambda + \frac{5}{12}.$$

The numerically computed eigenvalues are shown in Fig. 12 for $k_r = 3$ and three values of k_α. As k_α decreases, the method becomes stable. Interestingly, for the lowest value of k_α plotted, the Rossby wave amplitude is recovered but the dispersion errors are large.

b. Implicit free surface

Here, the method of DS94 is applied to the linearized QG equations. Their discretization is

$$\nabla^2\psi^{n+1} - \nabla^2\psi^{n-1} + 2\Delta t(\mu\psi_x^\beta + \delta^\mu) = 0, \quad (71)$$

$$\psi^{n+1} - \psi^n + \Delta t B^2 \delta^\theta = 0, \quad (72)$$

where the superscripts μ and θ refer to the equations given by Eqs. (48) and (49). This gives the characteristic polynomial

$$k_h^2(\lambda^2 - 1)(\theta\lambda + 1 - \theta) + 2F(\lambda)[\lambda - 1 - \Delta t i k \mu' B^2(\theta\lambda + 1 - \theta)] = 0, \quad (73)$$

where

$$F(\lambda) = \mu\lambda^2(1 - \mu - \gamma)\lambda + \gamma, \quad (74)$$

and can be written as

$$k_h^2/k_r^2(\lambda^2 - 1)(\theta\lambda + 1 - \theta) + 2F(\lambda)[\lambda - 1 - \Delta t i k/k_r^2 \mu'(\theta\lambda + 1 - \theta)] = 0. \quad (75)$$

DS94's optimal parameters are used in the comparison. The numerically computed results are shown in Fig. 13. DS94 and the α model have similar behavior for the Rossby waves. That is, the amplitude is recovered for large time steps, but the dispersion error increases.

6. Summary

It has been shown that the SW-α equations, which describe the slow-time dynamics of a rotating shallow water fluid, allow larger time steps than for the unaveraged SW equations. This is because the effects of the high wavenumbers are incorporated into those of the low wavenumbers through Lagrangian averaging. This effect appears in the linear analysis as a slow down of the frequency of the linear gravity waves at high wavenumber. The main result is an analytical estimate for the maximum allowable time step [Eq. (34)]. This estimate shows that as the grid is refined, the time step becomes independent of the mesh spacing and instead depends on on the length scale, α, a parameter of the model. Because of this result an analogy was constructed between the α model and time-implicit numerical methods through the use of the modified equation approach, and the α model was compared to the implicit method of DS94. The α model achieves a higher maximum allowable time step through the Lagrangian-averaged equations, while DS94 accomplishes a similar goal, but through its numerical formulation.

There are many remaining issues. First, I have reported that the linear analysis of the α model shows that the larger α, the larger the time step one may take and still retain numerical stability. The larger α, the more the small scales are being incorporated into the large. This is achieved in a novel way—through the Lagrangian-averaging process in Hamilton's principle. I have not reported on its ability to accurately model the mean fluid motion, but others have. The reader is referred to the introduction where I cite many investi-

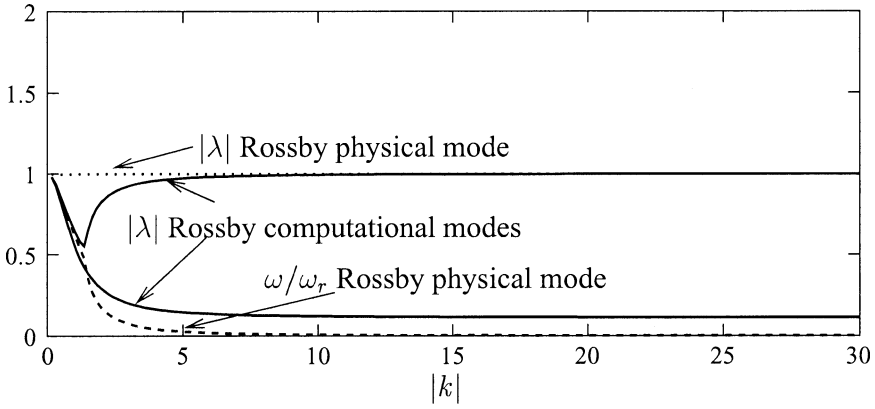

FIG. 13. Numerically computed amplitude and phase errors for DS94 for Rossby waves. The method is unconditionally stable, with no amplitude errors in the physical mode, but substantial phase errors.

gators' work. To elucidate the differences between the α model and implicit methods, I have compared it to the familiar numerical method of DS94. But having done so I would like to point out an issue of efficiency. Both DS94 and the α model rely on elliptic solvers. DS94 only needs one elliptic solver, while the α model requires two. This is not addressed in this work since for the linear case the elliptic problems can be solved exactly, but there is still a significant cost issue associated with the global elliptic solvers. This issue is currently being investigated in Geurts and Holm (2002, 2003), where a general theory for replacing the elliptic solvers with filters has been presented and tested for the large eddy simulations of shear layers. Second, even though I have not addressed the new nonlinearity of the α model, its effect on the solutions to the PDEs is significant, and therefore further investigation is needed. Last, there is a need for a technique to estimate its value. In the case of the SW-α, and other α models, there are many ways to do this.

The first approach is to physically measure α^2, which is the square of the correlation length of the Lagrangian trajectories. So far this approach has not lead to tangible results because of the difficulty of measuring Lagrangian trajectories in Eulerian numerical codes. The second is to compute α based on fluid stability, which is addressed in another work (Holm and Wingate 2004, manuscript submitted to *J. Phys. Oceanogr.*). And the last approach, described here, is to estimate α based on numerical stability.

The idea is as follows: α represents the smallest scale resolvable on a numerical mesh. Scales below α are swept by the fluid until they are damped by the numerical method (or other kinds of dissipation). Scales larger than α are more faithfully represented. Therefore, one approach chooses the smallest α that leads to numerical stability. In fact, one might call this an "artificial dispersion" method in which we solve Eq. (40) for α^2:

$$\alpha^2 = \frac{\Delta t^2 k_h^2 - \overline{Q}^2}{\overline{Q}^2 k_h^2} = \frac{Q^2 - \overline{Q}^2}{\overline{Q}^2 k_h^2}. \tag{76}$$

This equation can be used to compute α depending on the desired time step. For example, if one wants to use a CFL number of $Q = 2$ in a simulation, but desires an accuracy of $\overline{Q} = 1/2$, and has enough mesh points to support a maximum wavenumber of $K = 30$, then one calculates $\alpha = 0.129$. Implicit time differencing also controls dispersion and amplitude errors through the choice in time step.

Acknowledgments. The author would like to thank John Dukowicz, Ed Caramana, and Mark Taylor for their insightful remarks.

REFERENCES

Andrews, D. G., and M. E. McIntyre, 1978: An exact theory of nonlinear waves on a Lagrangian-mean flow. *J. Fluid Mech.*, **89,** 609–646.

Canuto, C., M. Hussaini, A. Quarteroni, and T. Zang, 1988: *Spectral Methods in Fluid Dynamics.* Springer-Verlag, 559 pp.

Caramana, E., 1991: Derivation of implicit difference schemes by the method of differential approximation. *J. Comput. Phys.*, **96,** 484–493.

Chen, S. Y., C. Foias, D. D. Holm, E. J. Olson, E. S. Titi, and S. Wynne, 1998: The Camassa–Holm equations as a closure model for turbulent channel and pipe flows. *Phys. Rev. Lett.*, **81,** 5338–5341.

——, ——, ——, ——, ——, and ——, 1999a: The Camassa–Holm equations and turbulence in pipes and channels. *Physica D,* **133,** 49–65.

——, ——, ——, ——, ——, and ——, 1999b: A connection between the Camassa–Holm equations and turbulence in pipes and channels. *Phys. Fluids*, **11,** 2343–2353.

Domaradzki, J. A., and D. D. Holm, 2001: Navier–Stokes alpha model: LES equations with nonlinear dispersion. *ERCOFTAC Bull.*, March, 22–25.

Dukowicz, J. K., and R. D. Smith, 1994: Implicit free-surface method for the Bryan-Cox Semtner ocean model. *J. Geophys. Res.*, **99,** 7991–8014.

——, ——, and R. C. Malone, 1993: A reformulation and imple-

mentation of the Bryan–Cox–Semtner ocean model on the connection machine. *J. Atmos. Oceanic Technol.,* **10,** 195–208.
Fabijonas, B. R., and D. D. Holm, 2003: Mean effects of turbulence on elliptic instability in fluids. *Phys. Rev. Lett.,* **90,** 124501.
Foias, C., D. D. Holm, and E. S. Titi, 2001: The Navier–Stokes alpha model of fluid turbulence. *Physica D,* **152–153,** 505–519.
Geurts, B. J., and D. D. Holm, 2002: Leray simulation of turbulent shear layers. *Advances in Turbulence IX: Proceedings of the Ninth European Turbulence Conference,* Kluwer Academic, 337–340.
——, and ——, 2003: Regularization modeling for large-eddy simulation. *Phys. Fluids,* **15,** L13–L16.
Hirt, C. W., 1968: Heuristic stability analysis. *J. Comput. Phys.,* **2,** 339–355.
Holm, D. D., 1999: Fluctuation effects on 3D lagrangian mean and eulerian mean fluid motion. *Physica D,* **133,** 215–269.
——, 2002: Averaged Lagrangians and the mean effects of fluctuations in ideal fluid dynamics. *Physica D,* **2875,** 1–34.
——, and B. T. Nadiga, 2003: Modeling mesoscale turbulence in the barotropic double-gyre circulation. *J. Phys. Oceanogr.,* **33,** 2355–2365.
——, J. E. Marsden, and T. S. Ratiu, 1998: Euler–Poicaré models of ideal fluids with nonlinear dispersion. *Phys. Rev. Lett.,* **80,** 4173–4177.
Nadiga, B. T., and L. G. Margolin, 2001: Dispersive eddy parameterization in a barotropic ocean model. *J. Phys. Oceanogr.,* **31,** 2424–2531.
——, and S. Shkoller, 2001: Enhancement of the inverse-cascade of energy in the two-dimensional Langrangian-averaged Navier–Stokes equations. *Phys. Fluids,* **13,** 1528–1531.
Warming, R. F., and B. J. Hyett, 1974: The modified equation approach to the stability and accuracy analysis of finite-difference methods. *J. Comput. Phys.,* **14,** 159–179.